Advanced cascade control strategy applied to an indirect hybrid solar-gas dryer: numerical and experimental investigations

ZOUKIT Ahmed[a*], DOUBABI Hajar[b], SALHI Issam[c], ABDENOURI Naji[b]

[a]: MINES ParisTech, PSL University, Center for Processes, Renewable Energy and Energy Systems (PERSEE), CS 10207 rue Claude Daunesse, F-06904, Sophia Antipolis, Cedex, France.
[b]: CISIEV, Applied physics department, FSTG, University Cadi Ayyad, Marrakesh 40 000,
[c]: FEMTO-ST Institute, Univ. Bourgogne Franche-Comté, UTBM, CNRS, Rue Thierry Mieg, 90000 Belfort, France.

[*] Corresponding author

Email of corresponding author: ahmed.zoukit@mines-paristech.fr

Abstract: In this paper, a cascade control strategy is applied to control the temperature inside a hybrid solar-gas dryer. In order to use the dryer even at night and in unfavorable weather conditions, the drying chamber is heated by two systems. The first one is the solar air heater and the second one is the gas heater. The solar collector heater is relatively slow compared to the gas heating system. Static and dynamic studies were established and have revealed the nonlinear behavior of each dryer subsystem. The cascade control approach was developed to control the drying temperature at different setpoints in a temperature range of [50°C, 90°C] by managing the gas flow delivered to burners according to received solar energy. Simulation tests followed by experimental investigations have revealed that the proposed control strategy has been able to fulfill the desired dryer performances at different temperatures level, with a propitious steady-state error, reduced overshoot, and a fast transient settling time. Hence, for controlled temperatures at 60°C, 70°C, and 80°C temperatures, the following performances were respectively obtained: a steady-state error of 0.5%, 0.28%, and 1.28%, an overshoot of 2.6%, 4.1%, and 2.5%, and a settling time of 20 min, 18 min, and 30 min. The developed control approach has shown also an effective perturbance rejection during the dryer operation. The proposed control technique and the manufactured kit can be easily integrated into hybrid dryers

and it’s an adequate and compatible solution with solar dryers for a drying operation of wide agro-food products. This solution also makes it possible to optimize the energy consumption of the secondary source.

Keywords: hybrid drying, temperature control, cascade approach, solar-gas drying.

1. Introduction

The drying process is usually required to preserve food commodities, mostly for a long period. Further, manufacturing of some products, such as wood, handcraft (leather and ceramic fabrication), mineral processing, paper paws as well as plastic industry, takes place in different types of kilns with high temperatures. But, before these products are subject to high temperatures, drying is an important step to get them ready to be fired. Thus, drying represents a major factor in many industries [1-3].

Solar drying seems to be a viable low-cost solution, but it is intermittent and depends strongly on solar irradiation [4-8]. At night or on cloudy days, the product could be rehydrated and, in some cases, deteriorated (contains moisture) as the drying operation could not be finished. Hence, the operator has to remove the product at night and put it in a safe moderate temperature area before spreading it again the next day. Therefore, it becomes imperative to involve auxiliary energy sources to keep a better and continuous drying process at the same temperature level.

A hybrid solar-gas dryer may be considered as a viable alternative solution for using this technology on a larger scale [9-11]. The hybridization leads to the control of the drying air conditions throughout the drying time regardless of the weather conditions. This form of hybridization leads to ensures a continuity of the drying process until the end of the operation [12].

The drying temperature is the major parameter that affects the quality of the dried product. Hence, the control of the temperature inside the drying chamber is a paramount issue that should be established after conceiving the dryer [13,14].

A well-controlled temperature at its optimum level would lead to good quality, the maintenance of the color, and the initial structure of the dried products without cracking. In addition, it would reduce the energy required for the drying operation. For agro-food products, the quality is controlled according to nutritional value, color, flavor, ode, and taste. In fact, these parameters deteriorate when the drying temperature exceeds a specific temperature depending on the product [15].

During the drying operation, the system faces multiple possible disturbances. These disturbances act directly on the drying temperature which in certain unfavorable cases can be above the recommended value. Hence, it is important to ensure an appropriate environment for drying products using an advanced control strategy to maintain the drying temperature closer to the desired value over time regardless of all disturbances of the main stochastic parameters.

According to the literature study, many authors have applied classical temperature controller (ON-OFF) inside hybrid dryers [16-18]. At the same time, there is a perceived lack of works dealing with the hybrid dryer temperature control suitable to solar dryers, low cost, and with performances similar to those got by the advanced control technic.

The hybrid solar dryers are strongly nonlinear systems as their main operation depends on random parameters which are solar radiation, airflow, relative humidity, and so on. These stochastic parameters render the behavior of the dryer in terms of drying temperature unpredictable and very difficult to be controlled. Hence, a strong nonlinear control technic rather than the classic one-OFF and PI controllers should be used to control the temperature of such devices.

A literature study has been established in order to figure out the suitable nonlinear control method that should be adopted to well fulfill the temperature control requirements. According to the literature, several methods of nonlinear control could be applied depending on the structure of the system to be controlled, the required performances, and the available computational resources on which the control program would be implemented. The nonlinear control methods could be categorized into two main groups: Variable structure control (SCV) for instance adaptive control [19], robust control [20], and sliding mode control [21]. Each method of them could be applied depending on the available information about the system (state-space model, range of the parameters uncertainty, unknown system parameters, or the variability of the system parameters during the operation).and decentralized control such as the LMI and Takagi Sugeno fuzzy (TSF) methods [22].

Sometimes, several systems are difficult to be represented by mathematical models which means that the equations representing their behavior are complex and represent a high level of non-linearity. However, if a prototype of the system is readily available. In this case, passing through the identification process is a viable option to obtain a mathematical model of the system to be studied.

On the other hand, one of the most used techniques for controlling nonlinear systems with specific particularities is the cascade control strategy. It involves the use of two feedback loops with the output of one controller (the primary or master controller) providing the set point of a second controller (the secondary or slave controller). It is particularly useful in processes with two process variables that the secondary process variable is faster-responding than the primary process variable. Such a control method has given improved performances of the controlled systems and especially in the rejection of external perturbations [23-26].

In specific cases, and for materials with low thermal conductivity, a temperature gradient should be controlled to avoid significant distortion of the dried product. For instance, the temperature gradient must be about 6°C/mm to preserve the shape and the quality of dried carrot cubes [27]. In addition to temperature, the deployed power impact the drying parameters such as drying time, drying curves, drying speed, drying efficiency, and the final product quality. Instead, the feedback temperature control can be insured by following predefined variable power profiles which gives rise to product quality [28].

The temperature control is highly recommended to get homogeneous dehydration and avoid dark zones in the final dried product as was highlighted by Ricardo Lemos Monteiro & all [29] in the oil-free sweet potato drying work.

The surface is the seat of heat and mass transfer, as well as the color and decomposition of the compounds contained in the product to dry. Hence, the surface temperature control turns into an essential parameter to control for an efficient drying operation [30]. In this work, the authors use a lumped parameter model, based on experimental results, for both the drying process of apple slices as well as the automatic control functionality. The developed model enabled the prediction of overall drying time for different drying parameters applied and so, drying costs can be reduced.

A cascade control strategy is proposed, where the external controller regulates the air temperature in the solar collector by the flow of burnt gas by generating a reference from the internal controller. The manipulated variables are the opening of the valve and the flow of burnt gas. This method has already been applied to the temperature control of a refrigerated chamber, using a vapor compression refrigeration system [31].

By convection heating, the temperature gradient is more pronounced inside the product. However, from the air to the product surface, the temperature is relatively homogeneous, especially during the steady-state. In opposite to the microwave drying, the temperature at the

product surface is still a bit higher than the air one. In this case, high heat levels usually lead to unfavorable quality results in the dehydrated product if not corrected with a favorable inverse temperature gradient characteristic of microwave heating. [32].

To keep the temperature at the optimum level during the seed drying, J.B. Oliveira [33] uses an adaptive robust technique (known as Shunt Indirect Variable Structure Model Reference Adaptive Control) which led to an insensitive to external disturbances. This method gives satisfactory results, however, it uses a high frequency switching control signal which is not with some actuators and sensors. To overcome this limitation, the author suggests using intelligent control and optimum control methods embedded in microcontrollers.

The response time temperature measurement and control remain too low, independent of the used technic. In previous works, temperature prediction and control methods based on the BP neural network were adopted to anticipate the correction of temperature variations and to lower the response time [34]. The response speeds of the existing temperature measurement and control systems are too low.

In all these previous works, temperature control is often used by acting on a single conventional energy source. Also, in most cases, the response time of existing measurement and control methods is high enough for an adequate correction of the temperature in a time that does not lead to an overshoot of the tolerable temperature.

To benefit from solar energy in a hybrid system configuration, an auxiliary backup heater is strongly required. Hybridization allows the temperature level adjustment and a non-stop use of the dryer whatever the intermittence and climatic conditions. This secondary energy source also makes it possible to manage and optimize energy consumption.

The temperature control process is required to maintain the temperature close to the setpoint regardless of the variation of incident solar energy and regardless of all other possible

disturbances. Indeed, significant temperature variations have a strong impact on the quality of the products to be dried.

On an industrial scale, the cost of the temperature control system weighs a lot on the investment budget and their use requires experienced users. These constraints do not support the development of solar dryers supposedly inexpensive, easy to use, and require little maintenance. When the secondary heating system is based on gas combustion, the temperature control passes through the input signal, which induces a certain valve opening which makes it possible for the combustion gas injection. In this case, the temperature is directly related to the gas flow.

Given the hybrid drying systems properties and operation behavior, the cascade control strategy seems to be more suitable for this type of process. It can perform better than a traditional single measurement controller.

This work is devoted to enriching the scientific literature in the field of temperature control inside hybrid drying systems using advanced control methods. It mainly addresses three main points:

- The study the nonlinear behavior of the hybrid solar-gas dryer and figure out an efficient modeling method for predicting its behavior in terms of drying temperature. The proposed modeling method is based on identification techniques rather than complex mathematical methods. The identified model of the dryer is very practical for the control purposes rather than the mathematical model which is more useful for studying the thermal behavior of the dryer and for design purposes.
- The study of the feasibility of an advanced control strategy for temperature control inside the hybrid dryer which has never been applied for such drying systems. The proposed method has been adapted to the dryer system and has proven good results by simulation.

- The development of an experimental setup for the implementation of the dryer controller and conducting experimental validation tests. The control system was simply integrated into the dryer system with good suitability for such applications.

Unlike dryers commonly used in industry, the control of temperature fluctuations following disturbances gives rise to precision beyond 8% and a response time that exceeds 60 minutes. While the disturbances invoked by solar radiation are generally high intensities and quite sudden. The use of its dryers for sensitive products remains very limited or results in lower product quality at the end of drying.

The control can be implemented in a low-cost system and does not require advanced technology to ensure its proper functioning.

The main objective of this paper is to develop a control system for monitoring the temperature inside the drying chamber by acting on the gas flow as the input parameter. To do so, first, static and dynamic studies of the dryer system have been established in order to figure out and to accurately precise the behavior linearity of the dryer. Second, the overall behavior of the dryer has been subdivided into two subsystems, and each one of them has been studied individually. Finally, numerical tests followed by experimental validations of the temperature control at three set points including 60°C, 70°C, and 80°C have been performed. These values are part of the favorable temperature range and are often encountered for drying agro-food products.

2. Materials and methods

2.1. Description of the hybrid solar-gas dryer prototype

A synoptic of the dryer alongside a pictorial view of the dryer prototype is presented in figures 1 and 2.

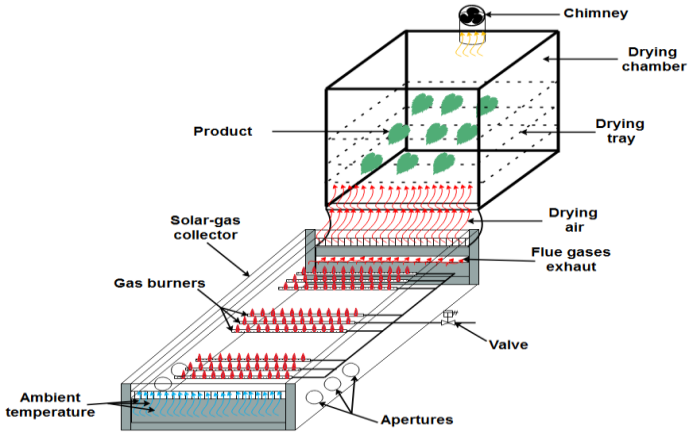

Figure 1. A synoptic of the hybrid solar-gas dryer

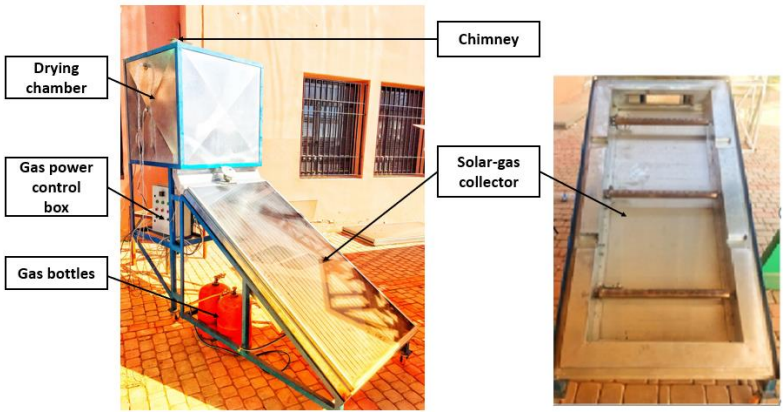

Figure 2. A pictorial view of the hybrid dryer

The dryer operates mainly with solar energy, while gas energy is used as an auxiliary heating system to indemnify the continuity of the drying process in the absence of solar energy and to control the chamber temperature as well [11]. The auxiliary heating system is composed of two gas bottles as an energy source, a proportional valve for gas flow control, and tubular burners for heating the drying air. The actuator is the proportional valve combined with the middle burner [35]. The constructing equipment and the user apparatus for the dryer study are presented in detail in the section that follows.

2.2 Apparatus and sensors

2.2.1. Gas burner

The gas burner is a natural tubular gas burner (30 mbar). The device produces a controlled flame by mixing fuel gas (butane gas) and the ambient air as an oxidizer and allowing for heating the drying air. It is made from an aluminized tube. The burner is supplied with an

injector. The diameter of the injector orifice is 1.3 mm. The burner length is 65 cm and its diameter is 5 cm. It is drilled with 15 holes for producing the flames. The power range of the burner is [2kW - 6.5 kW]. The real picture of the used burner is depicted in figure 3.

Figure 3. Tubular gas burner.

The used gas consists essentially of butane (C_4H_{10}) as a Liquefied Petroleum Gas (LPG) liquefied under pressure (since 1.7 bars). The gross calorific value (GCV) of butane is 13.7 kWh/kg and its combustion power is about: 29.5 m3/m3. The main chemical reaction that occurred during the gas combustion is written as follows:

$$C_4H_{10}(g) + \frac{13}{2}O_2(g) \rightarrow 4CO_2(g) + 5H_2O(g) \qquad \Delta H=-2658.2 \text{ kJ/mol}$$

2.2.2. Electrical ignitor

The ignition system is a device inserted in the head of the tubular burner. It produces a high-voltage output of about 500V which generates a spark with a special high frequency of about 30kHz. The generated spark is used further to ignite the gas-air mixture and provide the flames. A photo of the used ignitor is presented in figure 4.

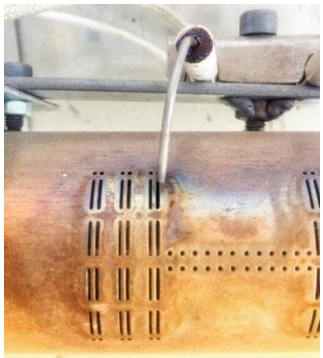

Figure 4. Electrical ignitor.

2.2.3. Flame sensor and the electrical valve

The flame detector is a sensor designed to detect the presence of a flame. It is installed in the head of the burner. The type of used flame detector in the burners is ionization current flame detection. After ignition, the intense ionization within the body of the flame is measured through flame rectification phenomena, whereby AC current flows in one direction when a voltage is applied. This current is used to verify the flame presence and quality. The real picture of the used flame sensor is presented in figure 5. The electrical valve is used in the input of the burner. It is a type SYPC with the ref: 2W-025-08. It is a safety valve used to manage the flow of gas energy fed to the burner within a piping system. It is supplied by 220 V as presented in figure 6.

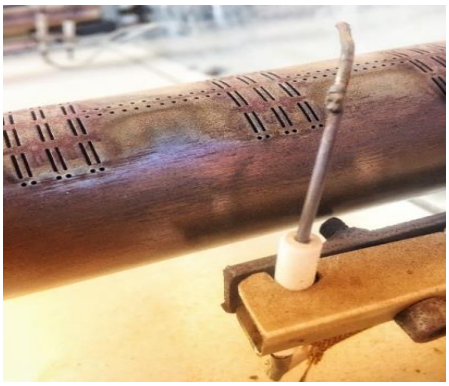

Figure 5. Flame sensors.

Figure 6. ON-OFF valve.

2.2.4. Security system

The security system that manages the burning process is an electronic box type BRAHMA (see figure 7). The used electronic box monitors safely the ignition of the burners, and the opening

of the safety valve feeds the burners with butane gas in normal operation and ensures the deactivation of the gas system in case of operation failure.

Figure 7. Security box.

2.2.5. Air vents

The solar gas collector is fitted with two vents allowing the entrance of the necessary air for combustion. The size of both openings is (45 cm × 10 cm). One opening is set on the front side and the other on the rear side of the collector. Each opening is fitted with an adjusted small door allowing the regulation of the amount of air that should be used for combustion. By a suitable opening of the door, high quality of flame is ensured, see figure 8.

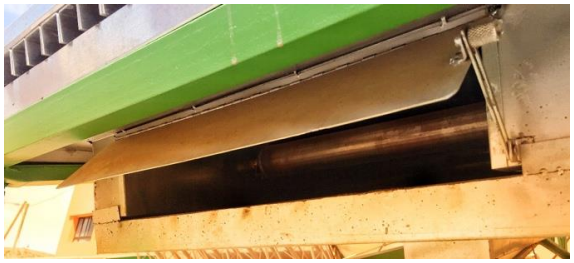

Figure 8. Air vent for gas combustion.

2.2.6 Gas power control box

The gas power control box includes all the temperature and relative humidity sensors in addition to the security system that manages the burning process. It includes three temperature sensors (TM-110 pt100, ±0.5°C), two relative humidity sensors (HM-110, 0.5%), and three gas security boxes. It also includes three switches type ON-OFF controlling each burner, three green lights indicating the normal operation of each burner, and three red lights informing about the default operation of the burners. Photos of the control box are depicted in figure 9.

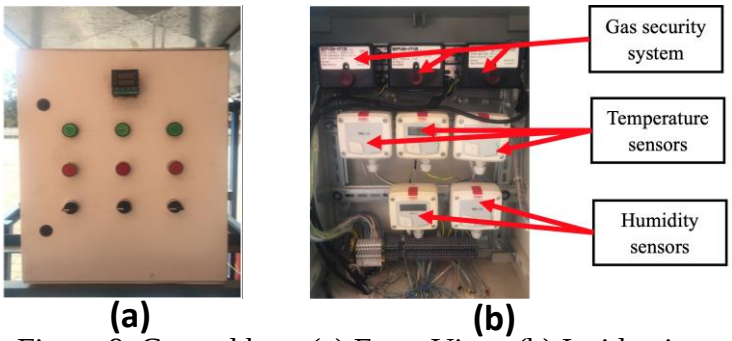

Figure 9. Control box. (a) Front View, (b) Inside view.

2.2.7. Gas proportional valve

The solar gas collector is fitted with a proportional valve (see figure 10) used to vary the gas flow delivered to the gas burners. The valve is supplied by 24VDC and controlled via a current signal in the range of 4-20 mA.

Figure 10. Gas proportional valves.

2.2.8. Gas flow meter

The used gas flow meter is type Kimo (90 lt/min, 16 bars, ± 4%). It is installed in the main gas pipe to measure the quantity of whole gas flow fed to the burners (see figure 11).

Figure 11. Gas flow meter.

2.2.9. Sensors

In order to perform the control of the dryer temperature, two types of sensors are used for acquiring the information delivered by the dryer, which is the temperature (TM-110 pt100, ±0.5°C) and gas flow, see figure 12. The ambient temperature and ambient relative humidity were recorded using a local weather station (Vantage Pro2). Incident global solar irradiation was measured locally using a Keep and Zonen pyranometer (a sensitivity of $14.69.10^{-3}$ mV). This latter is provided with adjustable inclination support to get the pyranometer at the same tilt angle of 30° from the ground level as the solar-gas collector. Both the solar collector and the pyranometer are directed to the south (with respect to the latitude of where the experiments are taking place, city: Marrakesh, country: Morocco).

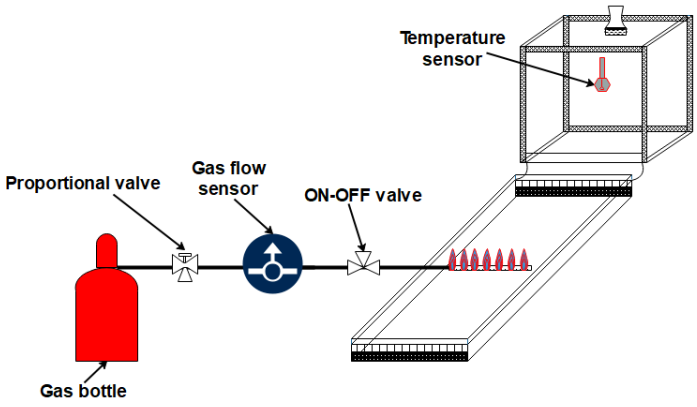

Figure 12. Sensors' placement in the hybrid dryer.

2.2.10. Data acquisition system

All experimental measurements were recorded by using a data acquisition platform that includes an automate type NI-cRIO-9030, LabVIEW software, and a touch panel host computer (figure 13).

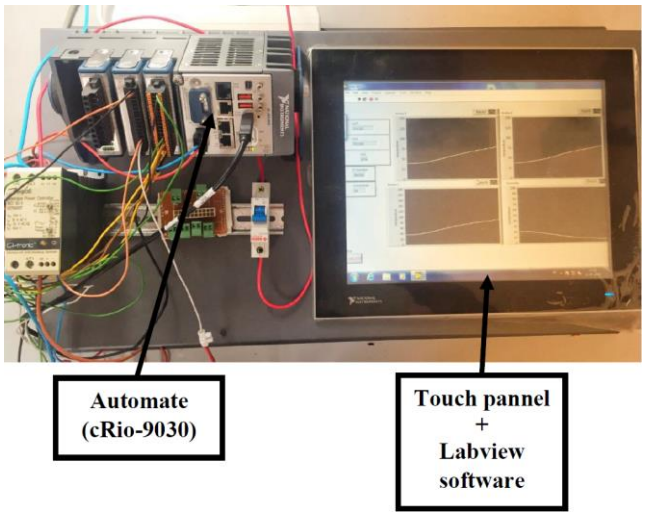

Figure 13. Data acquisition system.

For signals' compatibility consideration, DC current of 4-20 mA is used to control all actuators and delivered from all sensors. The temperature sensors were placed at three positions (bottom, middle, and top) inside the drying chamber.

2.3 Methodology

The nonlinearity in solar dryers is proved in previous works either by experimental tests and by a mathematical model [6]. In this work, the non-linearity of the considered system was highlighted by establishing the static and dynamic characteristics of the dryer. In order to achieve efficient temperature control, the overall system (hybrid solar-gas dryer) has been subdivided into two subsystems, where subsystem (S1) includes the proportional valve + middle burner, and subsystem (S2) is the collector and the drying chamber. A static and dynamic study of each sub-system has been set up in order to figure out their behavior. Based on the studies' results, it turned out that both subsystems showed a nonlinear behavior type threshold and saturation. Besides, the dynamic of both subsystems showed a big difference in terms of settling time. Taking into consideration the obtained information about the dryer subsystems, and since the developed dryer represents a new type of system to be controlled, the cascade control strategy seemed to be more adequate to perform efficient temperature control inside the drying chamber.

3. Study of the hybrid solar-gas dryer system control components

3.1. Input-output of the dryer system

The temperature inside the drying chamber can be considered as the output parameter of the studied dryer. This temperature can be affected by the change of each of these three variables: solar irradiation, ambient temperature, and the control signal of the proportional valve. In this system, solar irradiation is a variable that cannot be controlled, and so it can be considered as a measured disturbance. The ambient temperature influences only the initial temperature of the chamber, so it can be considered as a continuous component (Offset) [7]. The only controllable input is the control signal of the proportional valve. The block diagram of the system could be presented as shown in figure 14.

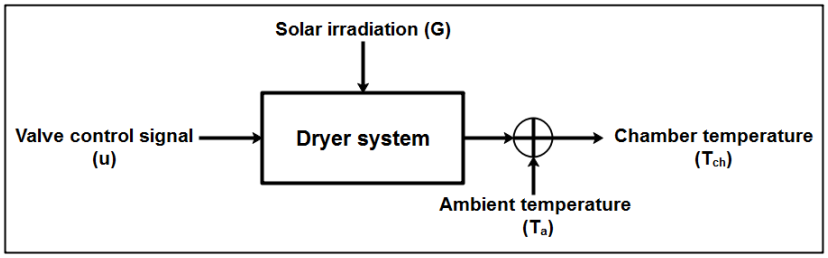

Figure 14. Reduced block diagram of the dryer system.

3.2. Characterization of the actuator components

The used actuator is composed of a gas proportional valve, an ON-OFF security valve, and the burner as shown in figure 15. The ON-OFF security valve is always maintained active (ON mode) when the actuator is operated; Hence, only the proportional gas valve and the burner can be considered for the characterization.

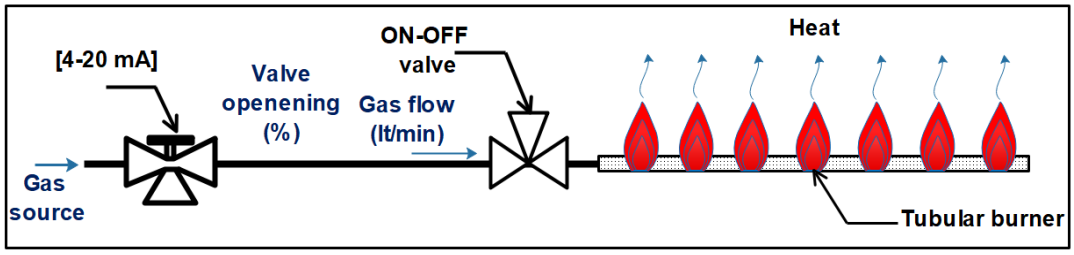

Figure 15. Scheme of the actuator.

The gas proportional valve is the main component used to adjust the quantity of gas flow consumed by the burner, thus, to maintain the temperature inside the drying chamber. It is

controlled by a current signal in the range of [4-20] mA. The used proportional valve is a type of motorized ball valve. A static test of the valve (working independently from the burner) is established to represent its characteristics. The latter is presented in figure 16. The characteristic is plotted by controlling the valve with a control signal in the range of 4-20mA and recording the opening percentage (with an accuracy of about 1%). It can be seen from figure 16 that the valve characteristic is indeed linear.

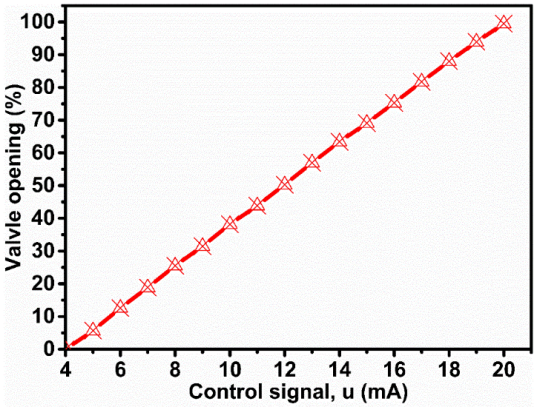

Figure 16. Characteristic of the valve.

The dynamic characteristic of the valve is also established as shown in figure 17. This test is carried out by applying steps of the control signal for the opening and closing of the valve. Then, the opening percentage is plotted versus time. An observation of figure 17 shows that for an applied control signal, the valve is opened or closed within a time delay of 3s.

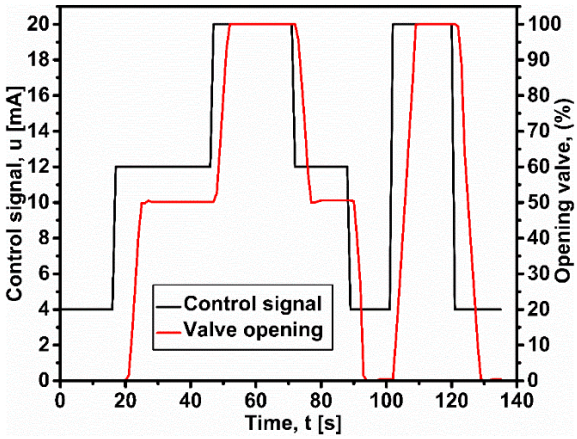

Figure 17. Profile of the dynamic behavior of the valve.

The burner is the main component that is responsible for providing heat to the drying air. When a suitable amount of gas flow is provided, the burner can normally operate. In standard

conditions (surrounding temperature of 25°C), the minimum working gas flow is 3.2 lt/min, and the maximum consumed gas flow is 14.3 lt/min.

3.3. Subsystems of the hybrid solar-gas dryer

The dryer system can be subdivided into two subsystems: subsystem (S1) and subsystem (S2). The subsystem (S1) consists of the valve and the burner. This latter has the valve control signal as an input and the gas flow as an output. The subsystem (S2) is the collector combined with the drying chamber which has the flame heat (gas flow) as the input and the drying temperature as the output. The block diagram is shown in figure 18.

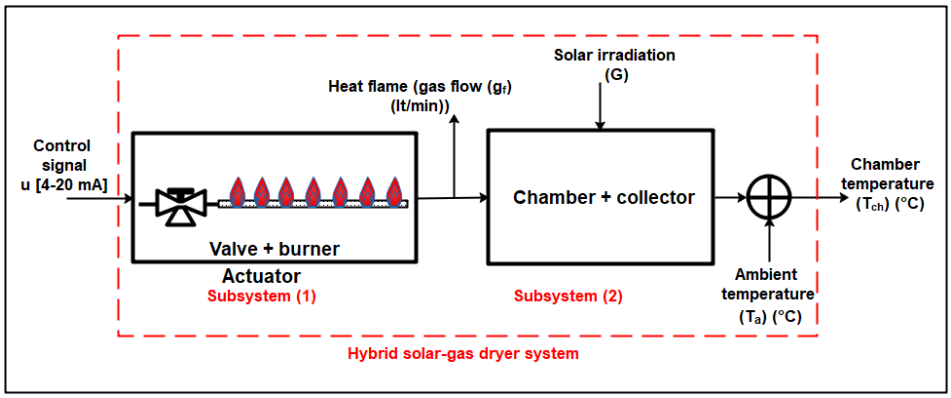

Figure 18. The schematic block of the dryer subsystems (S1) and (S2).

3.3.1. Static study of the subsystems

3.3.1.1. Subsystem (S1): valve and burner

The static study of the subsystem (S1) consists of establishing the static characteristic of the valve and burner when used together. The control signal of the proportional valve is varied in the range of 4-20 mA. For each control signal, the gas flow consumed by the burner was instantly recorded at about 4%. The static characteristic of the subsystem (S1) is shown in figure 19.

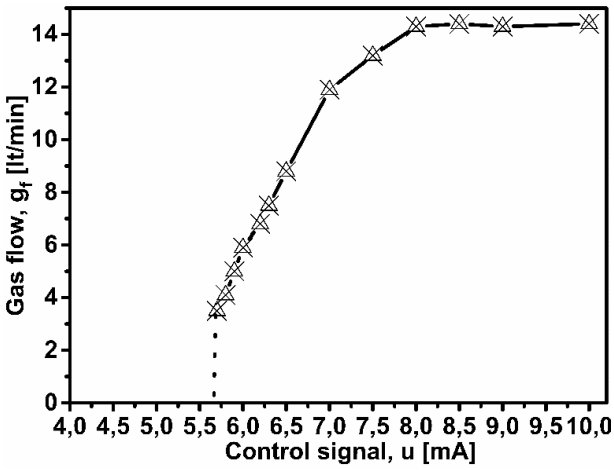

Figure 19. Static characteristic of the subsystem (S1): valve and burner.

An observation of figure 19 shows that the gas flow rate is consumed by the burner only for a control signal above 5.7 mA. In fact, after several tests, it was noticed that the minimum working gas flow (3.2 lt/min) is obtained with a valve control signal in the range of 5.6-5.8 mA depending on the ambient temperature of the surrounding air and the state of charge of the gas bottles. But, to ensure the minimum gas flow for the burner, a control signal of 5.7 mA is recommended. The behavior of the system can be considered linear when a control signal varies between 5.7 mA and 8 mA. Beyond the control signal of 8 mA, the opening of the valve does not have any effect on the gas flow, and it can be said that the system shows saturation. According to this study, it can be deduced that the overall behavior of the subsystem (S1) is non-linear and the type of non-linearity is a threshold (dead-zone) and saturation.

3.3.1.2. Subsystem (S2): Collector and drying chamber

The flame heat is proportional to the gas flow feeding the burner. Thus, the gas flow can be considered as a measured input variable for the subsystem (S2). In this regard, the static characteristic of the subsystem (S2) was established by measuring the average temperature within the drying chamber according to different gas flow rates. The experimental measurements were carried out in the permanent regime and at nights with approximately the same climatic conditions (to neglect the effect of ambient temperature change and solar irradiation). The static characteristic is shown in figure 20.

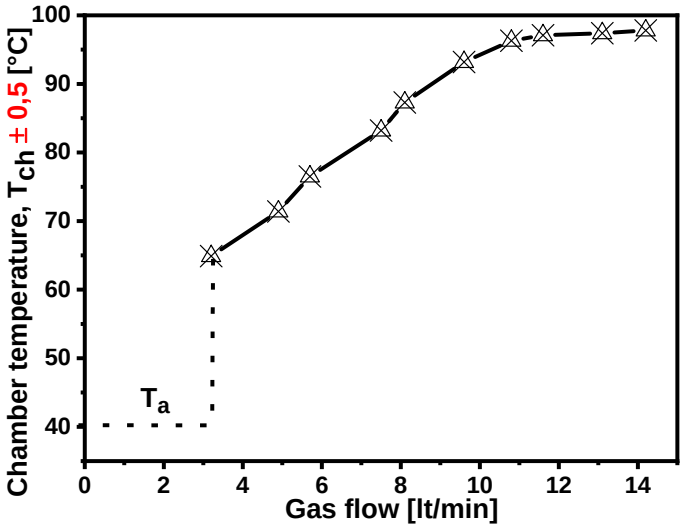

Figure 20. Static characteristic of the subsystem (S2): drying chamber.

It can be seen from figure 20 that the subsystem (S2) has a nearly linear behavior for a gas flow varying from 3.2 lt/min to 12.1 lt/min which corresponds to a temperature range of 65.1°C to 97.3°C. The overall behavior of this subsystem is non-linear type threshold and saturation.

3.3.2. Dynamic study of the subsystems

3.3.2.1. Dynamic characteristic of the subsystem (S1)

The dynamic study of the subsystem (S1) consists of controlling the proportional valve with step signals and recording the gas flow profile in a transitory state. To do so, two-step control signals varying from 4 mA to 6.7 mA and then to 7.2 mA were applied to the valve. The whole duration of the experiments is 100 s. Figure 21 depicts the control signal of the valve and the gas flow evolution versus time. An observation of figure 21 shows that the subsystem (S1) has a fast dynamic with an average settling time of 2 s.

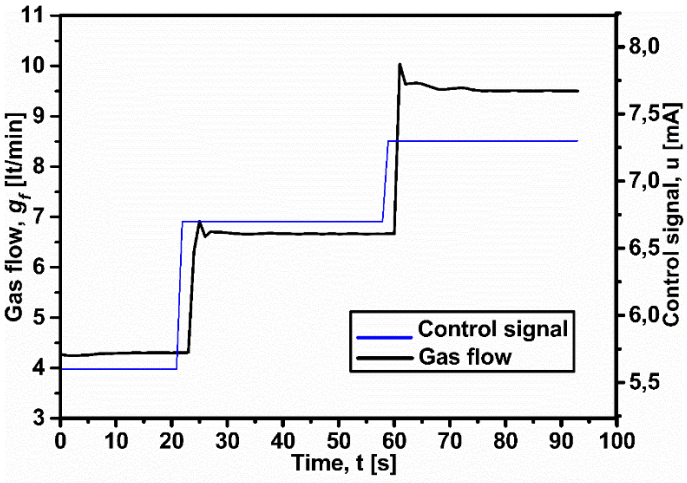

Figure 21. The control signals of the valve and gas flow evolution (4%).

3.3.2.2. Dynamic characteristic of the subsystem (S2)

The dynamic behavior of the subsystem (S2) consists of measuring the temperature inside the drying chamber at an input gas flow. An experimental test was carried out by feeding the burner with a gas flow of 14.3 lt/min. The temperature inside the drying chamber was recorded every 1 min at about ± 0.5°C for a working duration of 150 min. The temperature profile is given in figure 22 in which the temperature reached its maximum with a settling time of 68 min.

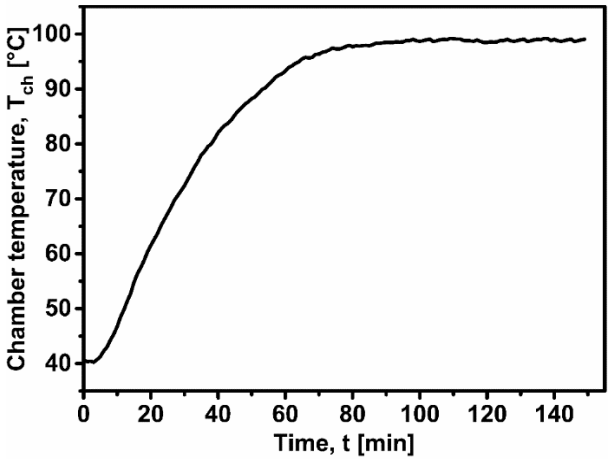

Figure 22. Evolution of the temperature profile inside the drying chamber.

4. Cascade control approach

4.1 PI controller for nonlinear system

In most cases where a system behavior represents a nonlinearity type dead-zone with saturation (three ways proportional valve); a PI controller with an anti-windup algorithm is widely used

for control purposes. The anti-windup algorithm [36] is used to avoid the magnification of the integral term of the controller caused by the saturation behavior of the controlled system.

The modified algorithm for the PI controller with anti-windup is as follows:

$$u(t) = S^{at}(K_p(s_{set}(t) - s_m(t)) + I(t)) \quad (1)$$

$$\frac{dI(t)}{dt} = K_i(s_{set}(t) - s_m(t)) + K_s(U - K_p(s_{set}(t) - s_m(t)) - I) \quad (2)$$

where:

$$\begin{cases} S^{at}(U) = U \ \ if \ \ Umin \leq U \leq Umax \\ S^{at}(U) = Umin \ \ if \ U \leq Umin \\ S^{at}(U) = Umax \ \ \ if \ U \geq Umax \end{cases}$$

$u(t)$ is the control signal, K_p is the proportional gain, K_i is the integral gain and $I(t)$ is the integral term of the PI controller, respectively, $s_{set}(t)$ is the desired value, $s_m(t)$ is the measured output of the system. Note that K_s must verify $K_s * K_p > K_i$.

4.2. Application of cascade technique for the dryer temperature control

According to the dynamic study of the subsystem (S1) and subsystem (S2), it can be noticed that there is a big difference between both subsystems' dynamics. The subsystem (S1) has a fast dynamic (gas flow variation) with a settling time of 2 s while the subsystem (S2) has a slow dynamic with a settling time of 4080 s. It can be inferred that the dynamic of the subsystem (S1) is 2720 times faster than the one of the subsystem (S2). Given these aforementioned properties, a cascade control strategy seems to be more suitable for this kind of process [37-39]. It can ensure better performances than traditional single measurement control. The main advantages of the cascade control strategy are to provide efficient control of the dryer temperature with fast setpoint changes and external disturbances rejection.

The proposed cascade strategy is composed of two loops: an outer and an inner loop. The schematic of the block diagram of the cascade control strategy is presented in figure 23. Given an external reference T_{chref} and once T_{ch} is measured, the outer loop computes, using a controller noticed C_2, the required gas flow as control action. This reference must be tracked by the inner

loop using the controller C_1 which manipulates the proportional valve so that this latter satisfies the gas flow imposed by the outer loop.

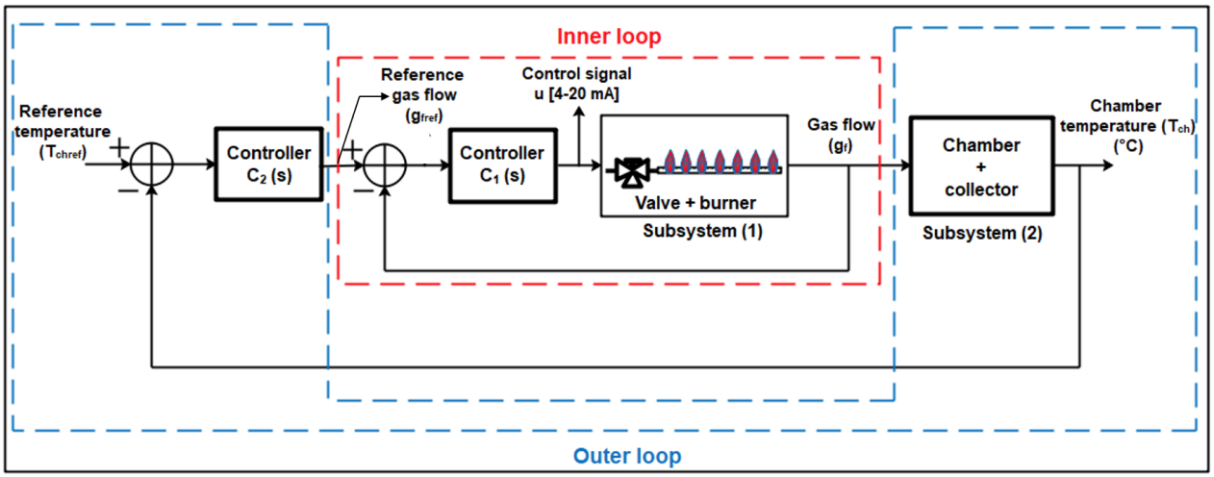

Figure 23. Block diagram of the proposed cascade control structure.

The variable g_f is called the intermediate variable. It is a variable in time advance of the T_{ch} measurement variable. If there is a change in the control signal 'u', or a disturbance affecting the subsystem (S1) such as the change in gas flow through a change in the opening or closing of the gas bottles, the state variable g_f will be the first to be affected before the measurement variable T_{ch}. In the conventional control loop, the controller does not begin to react to correct the effect of a disturbance until it is informed once the measured T_{ch} is changed. While with the used cascade structure, if a disturbance affects the subsystem (S1), it will be supported by the inner loop. This loop must be well sized so that it is fast, and so the effect of the disturbance can be neutralized without the appearance of a significant impact on the drying temperature.

4.2.1. Design of the inner controller

4.2.1.1. Subsystem (S1) identification

To identify the transfer function of the subsystem (S1) (valve and burner), a variation of the control signal is applied around an operating point in the linear zone of the static characteristic presented in figure 19. A control step signal varying from 5.6 mA to 7 mA was applied to the proportional valve. The gas flow rate consumed by the burner is recorded as shown in figure 24.

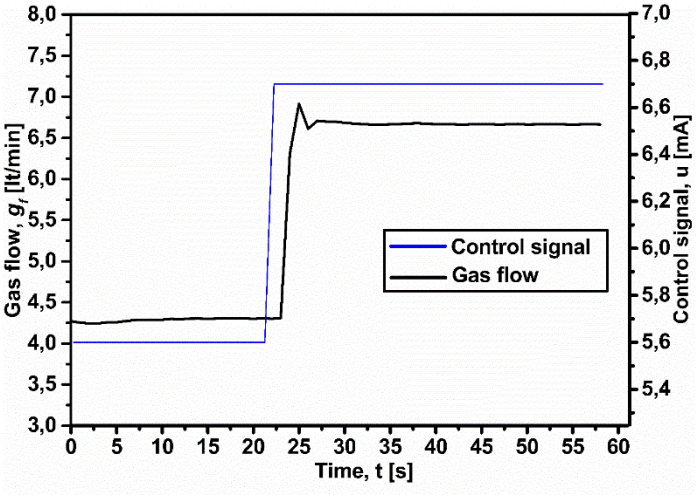

Figure 24. Step response of the subsystem (S1).

The outlet (gas flow) of the subsystem (S1) shows an overshoot before it stabilizes in the steady-state. To identify the linear model of the subsystem (S1), the System Identification function '*Ident*' presented on Matlab was used.

The obtained model by the *Ident* function is a transfer function of order 3 (Eq. 3). The simulated output obtained by the model fitted the measured signal with a fitting percentage of 98% (see figure 25).

The obtained transfer function is as follows:

$$H_1(s) = \frac{5.802s+33.71}{s^3+5.643s^2+14.45s+19.93} \quad (3)$$

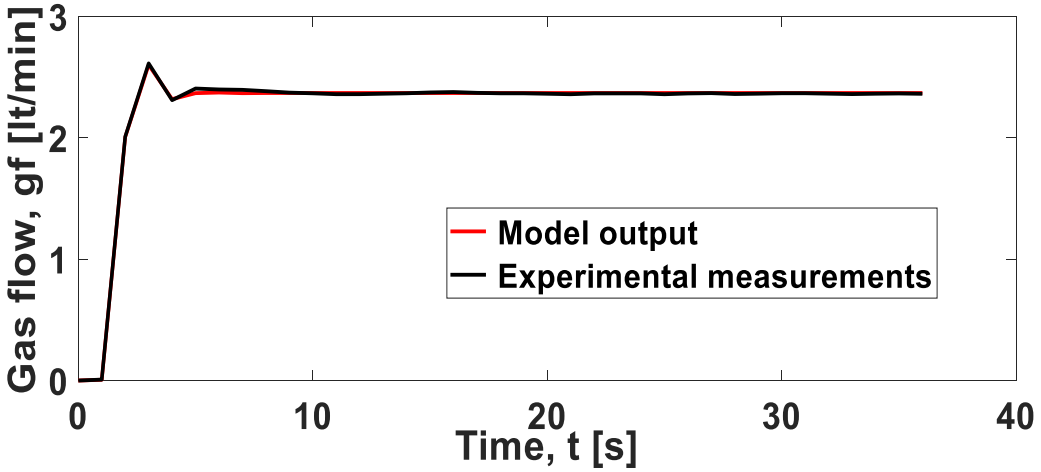

Figure 25. The model identification of the subsystem (S1).

4.2.1.2. PI controller for the subsystem (S1)

The control equations of the PI controller are written as follows:

$$u(t) = K_{p1}\left(g_{fref}(t) - g_{fm}(t)\right) + I(t) \quad (4)$$

$$\frac{dI(t)}{dt} = K_{i1}\left(g_{fref}(t) - g_{fm}(t)\right) \quad (5)$$

The used proportional valve is a three-way valve. Using the PI controller, the algorithm commonly used with this type of valve is as follows:

- For u < 5.3 mA, the burner does not operate and the drying chamber temperature is close to the ambient one.
- For u > 8 mA, the burner is operating at full power and the chamber temperature reaches its maximum.
- For the intermediate values of u ∈ [5.3 mA ,8 mA], the drying chamber is partially heated with an intermediate temperature.

The above-mentioned PI equations (4 and 5) remain very limited and cannot work for this application. The reason is that the control signal 'u' must remain between 5.3 mA and 8 mA. To take these limitations into account, u is saturated and the obtained modified control law is the following:

$$u(t) = S^{at}(K_{p1}\left(g_{fref}(t) - g_{fm}(t)\right) + I(t)) \quad (6)$$

$$\frac{dI(t)}{dt} = K_{i1}\left(g_{fref}(t) - g_{fm}(t)\right) \quad (7)$$

Where S^{at}(u) = u if u ∈ [5.3 mA ,8 mA], S^{at} (u) = 5.3 mA for u < 5.3 mA and S^{at}(u) = 8 mA for u > 8 mA.

Considering the anti-windup mechanism, the following new control algorithm is achieved:

$$u(t) = S^{at}(K_{p1}\left(g_{fref}(t) - g_{fm}(t)\right) + I(t)) \quad (8)$$

$$\frac{dI(t)}{dt} = K_{i1}\left(g_{fref}(t) - g_{fm}(t)\right) + K_{s1}(u(t) - K_{p1}\left(g_{fref}(t) - g_{fm}(t)\right) - I(t)) \quad (9)$$

The gains K_p, K_i and the gain of the anti-windup K_s must verify:

$$K_{p1} > 0;\ K_{i1} > 0\ ;\ K_{s1} > 0 \text{ and } K_{s1} * K_{p1} > K_{i1} \quad (10)$$

The PI parameters are calculated by applying affine parametrization and considering certain conditions for robust stability using the PIDtune function provided by Matlab. This latter provides algorithms to synthesize PID controllers for linear and nonlinear plant models. It leads to tunes automatically the suitable parameters of the chosen controller to balance the performance (response time) and robustness (stability margin) of the controlled system. The functional organization of the inner loop is represented by the following diagram (see figure 26):

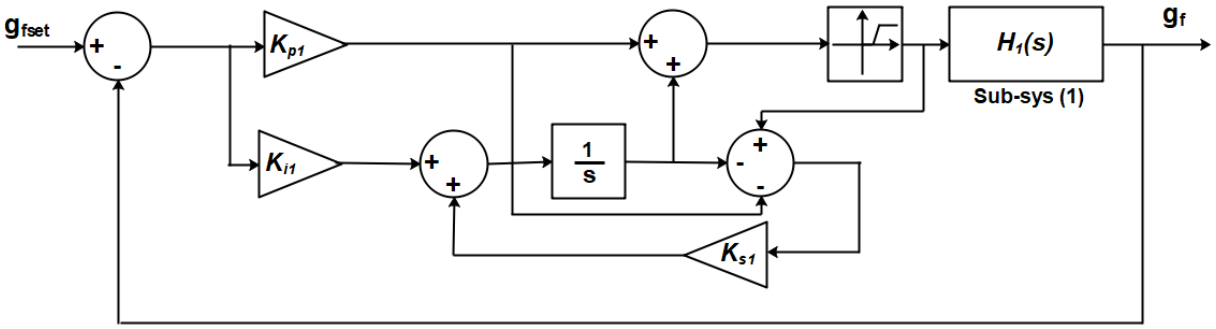

Figure 26. Diagram of the closed inner loop.

Matlab simulations have been developed for a control test and setpoint tracking test. The control test is performed to control the gas flow for a setpoint of 6.6 lt/min, and the tracking test is established to track the change in the gas flow setpoint from 8 lt/min to 5 lt/min. PI regulator parameters with anti-windup are shown in Table 1:

Table 1. Tuned PI parameters for the inner loop controller.

Parameter	Values	Errors
K_p	0.010	$\pm 10^{-3}$ (10%)
K_i	0.10	$\pm 10^{-2}$ (10%)
K_s	200	$\pm$ 5 (2.5%)

Simulation results are presented in figures 27a and 27b. According to the obtained results, the controller manages to stabilize the gas flow after 5 seconds with a static error equal to zero (see figure 27a). Moreover, the developed controller was able to ensure tracking of setpoint with desirable performance (figure 27b).

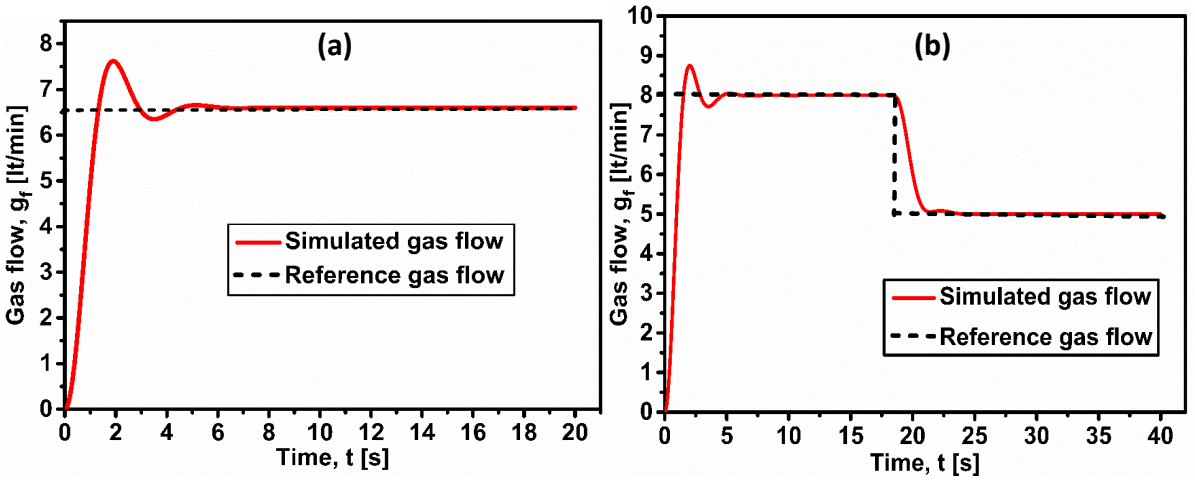

Figure 27. Simulation test of gas flow control; (a) control test; (b) tracking test of the gas flow.

4.2.1.3. Practical validation of the inner loop design

In order to validate the simulation results, a gas flow control test was carried out on the developed prototype. The same parameters of the PI controller with anti-windup that were used in the simulation study were also used in the practical test. Figure 28 shows the experimental results of the gas flow evolution during the dryer operation. The burner is operated with a consumed gas flow of 13.01 lt/min, then a control signal is applied to the proportional valve in order to control the gas flow at 4 lt/min for one minute. Then, the gas flow is controlled at the setpoints 6.6 lt/min and 10 lt/min in order to cover approximately the overall linear zone for subsystem (S1) operation. Figure 29 shows the control signal applied on the valve; it can be seen that the control signal remains in the range of [5.3, 8] mA. The control signal has small variations since the pressure of the gas bottles varies over time which affects the gas flow. In this regard, the control signal always has small variations in order to adjust the valve and maintain a constant gas flow.

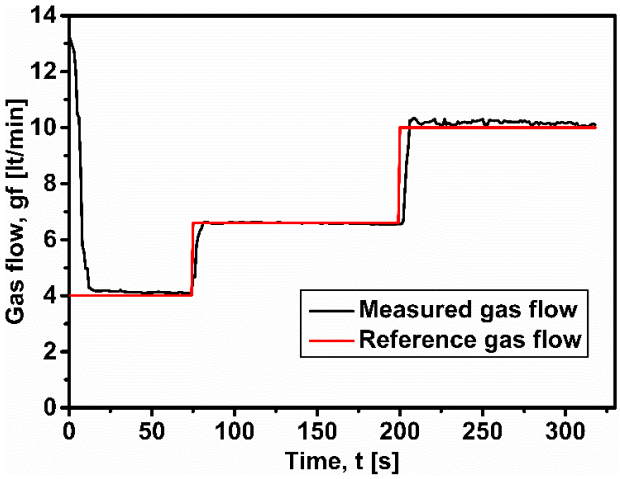

Figure 28. Experimental control test of the gas flow.

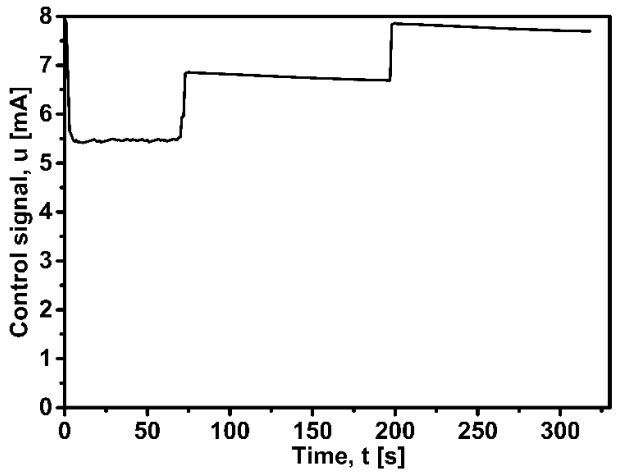

Figure 29. Control signal of the proportional valve.

4.2.2. Design of the outer loop controller

4.2.2.1. Subsystem (S2) identification

Identification of the subsystem model (S2) (drying chamber and collectors) is carried out by applying two control steps ‘u’ which will provide a gas flow included in the linear zone of its static characteristic and also in the linear zone of the static characteristic of the drying chamber. For this purpose, a gas flow of 5.5 lt/min is provided to the burner in order to raise the chamber temperature into the linear zone. Then, a step of gas flow varying from 5.5 lt/min to 10.1 lt/min is applied to the system for 5 hours. The temperature within the drying chamber was recorded with a time step of 1 min. The gas flow rate and drying chamber temperature are shown in figures 30 and 31, respectively.

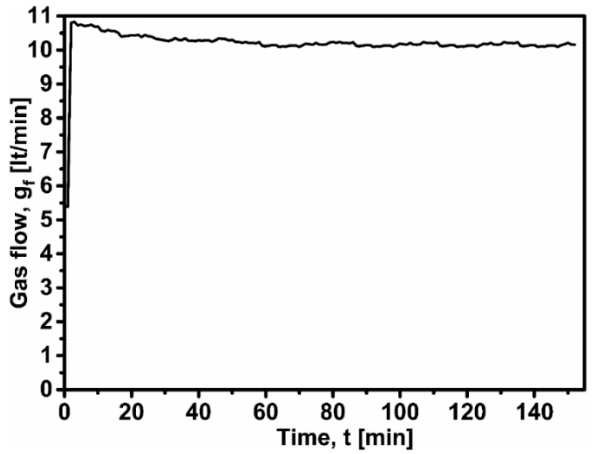

Figure 30. Step of gas flow from 5.5 lt/min to 10.1 lt/min.

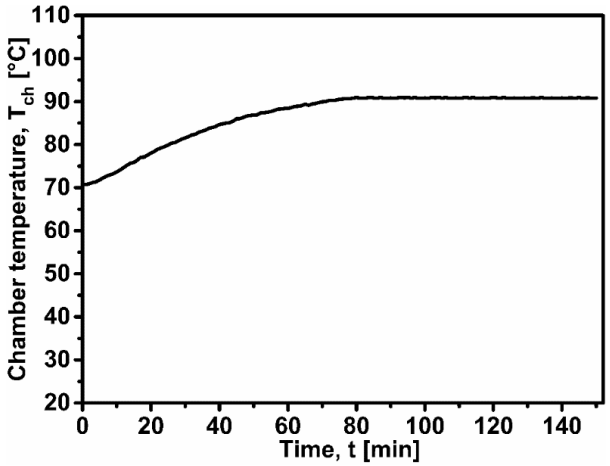

Figure 31. Temperature evolution inside the drying chamber.

The input (gas flow) and output (chamber temperature) signals' records are loaded into Matlab. The system identification function 'Ident' is used to develop an identified model of the subsystem (S2). The simulated output of the subsystem (S2) model fitted the measured temperature with 97% as shown in figure 32. The corresponding transfer function (denoted H_2) of the subsystem (S2) is as follows:

$$H_2(s) = \frac{0.001055s + 2.23e^{-6}}{s^2 + 0.001028s + 3.799e^{-7}} \quad (11)$$

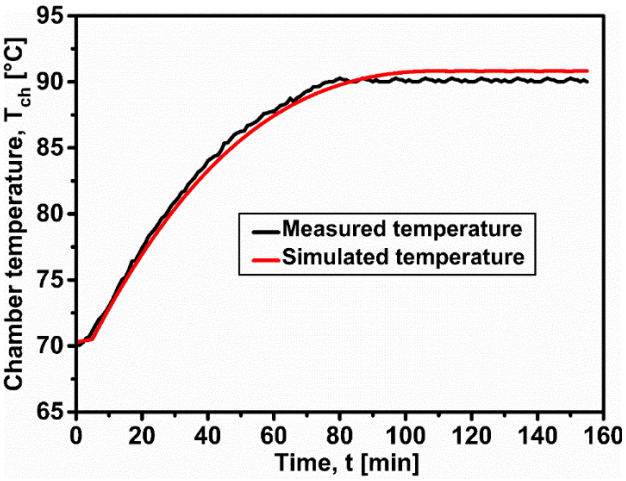

Figure 32. Comparison between the response of the identified model and the measured response.

4.2.2.2. PI controller for Subsystem (S2)

The behavior of the subsystem (S2) represents the same nonlinearity as the subsystem (S1). In this regard, the same type of PI controller (C_2) is adopted for temperature control inside the drying chamber. The PI controller for the subsystem (S2) will be designed to calculate the suitable gas flow to be maintained by the inner loop (controller C_1). The same PI algorithm used for the inner loop is adopted for the outer loop. The saturation function of the gas flow is as follows:

$$S^{at}(g_{fset}) = g_{fset} \qquad if \qquad g_{fset} \in [3.2\ lt/min\ ,14.3\ lt/min\ ] \tag{12}$$

$$S^{at}(g_{fset}) = 3.4\ lt/\min \quad if \quad g_{fset} < \ 3.2\ lt/min \tag{13}$$

$$S^{at}(g_{fset}) = 12.3\ lt/min \qquad if \qquad g_{fset} > 14.3\ lt/min \tag{14}$$

The following nonlinear PI control algorithm is:

$$u(t) = S^{at}(K_{p2}(T_{chref} - T_{chm}(t)) + I(t)) \tag{15}$$

$$\frac{dI(t)}{dt} = K_{i2}(T_{chref} - T_{chm}(t)) + K_{s2}(u(t) - K_{p2}(T_{chref} - T_{chm}(t)) - I(t)) \tag{16}$$

The gains K_{p2}, $K_{i2,}$ and the gain of the anti-windup K_{s2} must verify:

$$K_{p2} > 0\ ;\ K_{i2} > 0\ ;\ K_{s2} > 0 \ \text{ and } \ K_{s2} * K_{p2} > K_{i2} \tag{17}$$

The design of the outer loop controller is achieved by incorporating the inner loop which is already designed. The parameters of the outer loop PI controller were adjusted by applying an

affine parametrization using *PIDtune* function. The numerical investigations of the temperature control by the global loop including the inner and the outer loops are established. The used parameters of the controllers are summarized in Table 2.

Table 2. The controller's parameters of the global cascade control loop.

Outer loop controller			Inner loop controller		
Parameter	Value	Errors	Parameters	Value	Errors
K_{p2}	0.2	$\pm 10^{-3}$ (10%)	K_{p1}	0.01	$\pm 10^{-3}$ (10%)
K_{i2}	10^{-4}	$\pm 10^{-5}$ (10%)	K_{p1}	0.1	$\pm 10^{-2}$ (10%)
K_{s2}	300	± 6 (2%)	K_{s2}	200	± 5 (2.5%)

The simulation diagram of the global loop is illustrated in Figure 33.

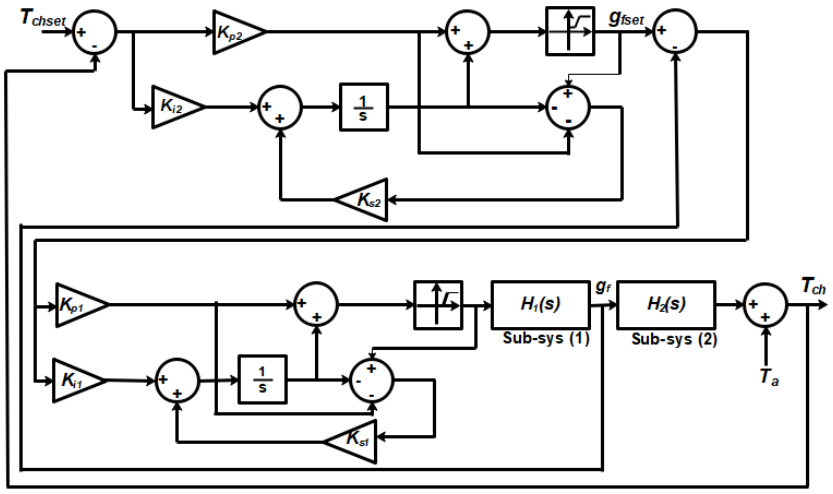

Figure 33. Global cascade control loop of the dryer temperature.

4.3. Simulation tests of the temperature control

Simulation tests of the temperature control at 60 °C, 70°C, and 80°C were conducted for 5 hours. The simulation results are shown in figures 34-39. It can be seen from the figures that the designed controllers were able to drive the chamber temperature to the reference ones (60°C, 70°C, 80°C) with a settling time of 36 min, 50 min, and 57 min, respectively. The dynamic response exhibits an overshoot of 2.6%, 3,2% and 1,7% with a steady-state static error of 1.3%, 0,28% and 0,6% for temperature control at 60°C, 70°C and 80°C, respectively (see figures 34, 36 and 38). Figures 35, 37, and 39 show the control signal delivered to the proportional valve.

An observation of these figures shows that the control signal is smooth and remains in the linear zone of the static characteristic of the valve and burner.

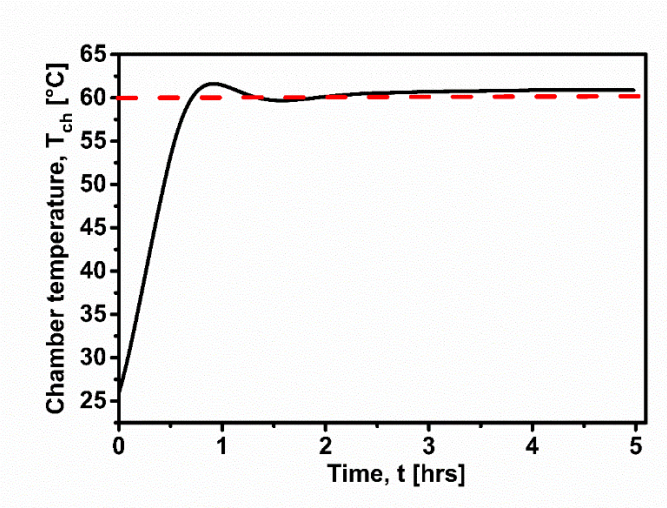

Figure 34. Simulated temperature control at 60°C.

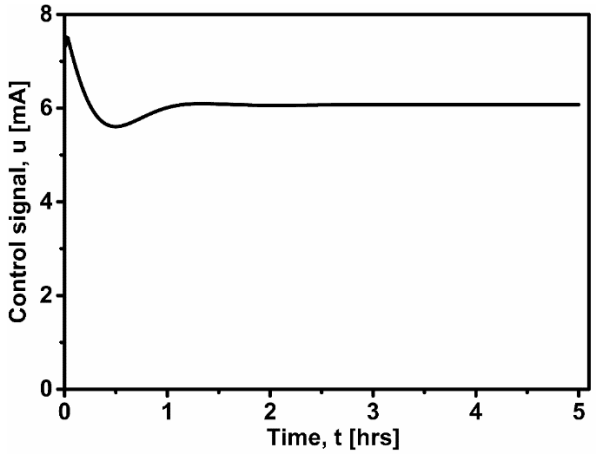

Figure 35. The control signal of the proportional valve for temperature control at 60°C.

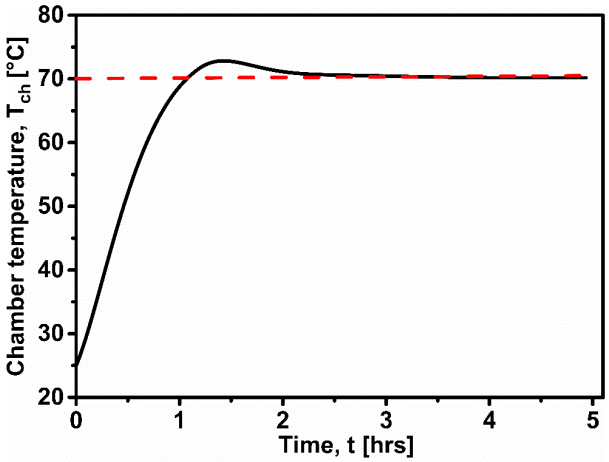

Figure 36. Simulation test of the temperature control at 70°C.

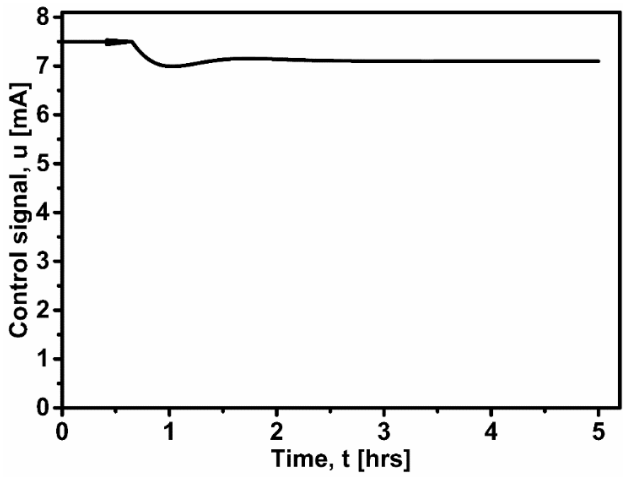

Figure 37. Control signal provided to the valve for the control test at 70°C.

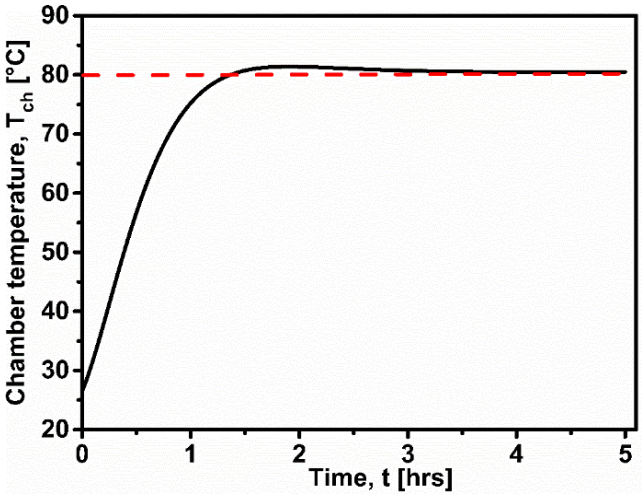

Figure 38. Simulated temperature profile for a control test at 80°C.

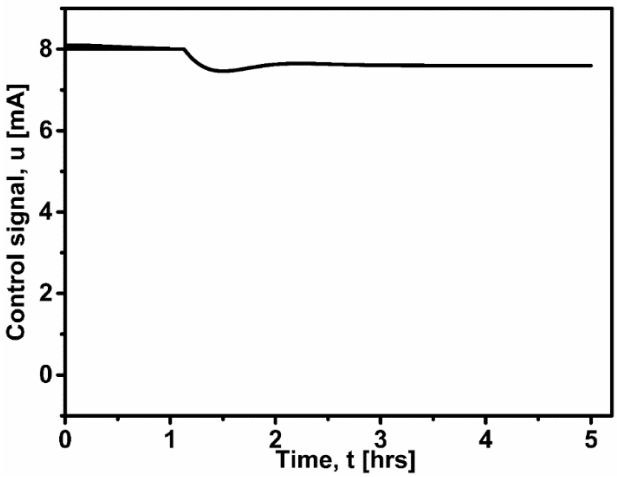

Figure 39. The control signal of the valve for temperature control at 80°C.

According to the obtained simulation results, it was concluded that the developed approach is suitable for temperature control inside the hybrid solar-gas dryer. The temperature was well maintained at the desired values with a settling time and steady error remaining under 57 min

and 3.2 %. Such performances are widely accepted and well fulfill the drying purpose requirements.

4.4. Experimental validation of the temperature control

The main focus in this section is to experimentally validate and evaluate the performances of the proposed temperature control approach. The parameters of the outer loop controller (C_2) and the inner loop controller (C_1) were set to the same values used in the simulation study. The cascade control structure was implemented using the controller NI-cRIO-9030. To evaluate the performances of the developed control strategy, four variables were sensed including the chamber temperature (T_{ch}), the consumed gas flow (g_f), the calculated reference gas flow (g_{fref}), and the control signal (u). The temperature is acquired with a sampling time of 1 min while g_f, $g_{fref,}$ and u were updated every 1 second. The tests were performed at night in order to cancel the effect of solar irradiation. Further, the wind speed is also measured using a weather station type (Vantage pro). The wind speed was taken into consideration because it is a parameter that affects the quality of the burner's flame and in consequence the transient behavior of the dryer.

4.4.1. Control at the temperature setpoint of 60°C, 70°C, and 80°C

The experimental tests were performed to investigate the ability of the developed controllers to maintain the drying temperature at 60°C, 70°C, and 80°C. The experiments were conducted on the days of 1st, 3rd, and 5th November 2021. The test was carried out within 5 hours starting from 6 pm to 11 pm. The ambient temperature remained approximately constant at 20°C during all the tests with a slight variation of 1°C. The climatological conditions during each control test are presented in tables 3, 4, and 5.

Table 3. Climatological conditions during the experiments for a control test at 60°C.

Day of experiment	November, 3rd, 2021
Average ambient temperature	20 °C
Wind speed	Max: 6.4 km/h Min: 1.6 km/h

Table 4. Climatological conditions during the experiments for a control test at 70°C

Day of experiment	November, 1st, 2021
Average ambient temperature	21.0±0.5 °C
Wind speed	Max: 1.6 km/h; Min: 0 km/h

Table 5. Climatological conditions during the experiments for a control test at 80°C

Day of experiment	November, 5th, 2021
Average ambient temperature	20.0±0.5 °C
Wind speed	Max: 6.4 km/h; Min: 1.6 km/h

The controlled temperature profiles are presented in figures 40, 41, and 42. It can be seen that the temperature is well maintained at 60°C, 70°C, and 80°C with a settling time of 20 min, 18 min, and 30 min, respectively. The temperature is set to the references with static errors of 0.5 %, 0,28%, and 1,12% while the dynamic responses exhibit a small overshoot of 2.6 %, 4,1%, and 2,5 % for the temperature control at 60°C, 70°C, and 80°C, respectively. The variation of the overshoot value depends on different parameters such as the temperature level and more precisely the climatological conditions including the wind speed which affect the quality of the flame and so the heat quantity transferred to the heat exchanger. The ambient temperature which affects the initial temperature inside the chamber and also the solar irradiation which is considered as a source of heat for the dryer. All these parameters are random and cannot be controlled which leads a huge difficulty to get the same temperature response for the dryer. The performances of the control approach are depicted in Table 6.

Table 6. Control approche performances.

	Reference temperature		
	60°C	70°C	80°C
Control performances			
Static error	0,5%	0,28%	1,12%
Overshoot	2,6%	4,1%	2,5%
Settling time	20 min	18 min	30 min

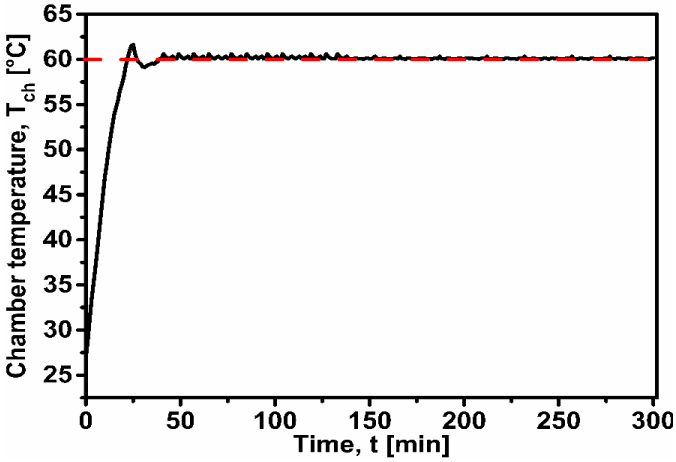

Figure 40. Experimental profile of the controlled temperature at 60°C.

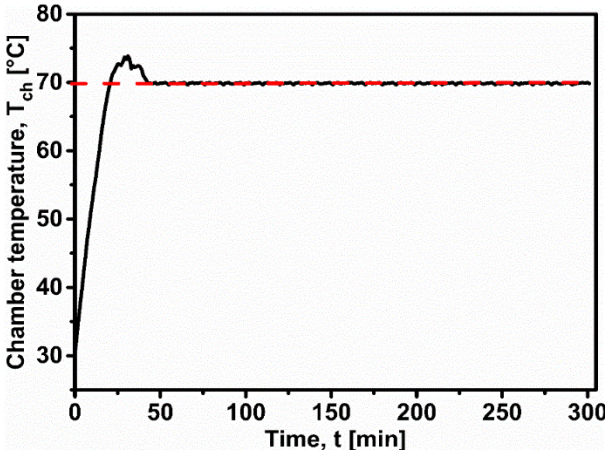

Figure 41. Experimental temperature evolution for a control test at 70°C.

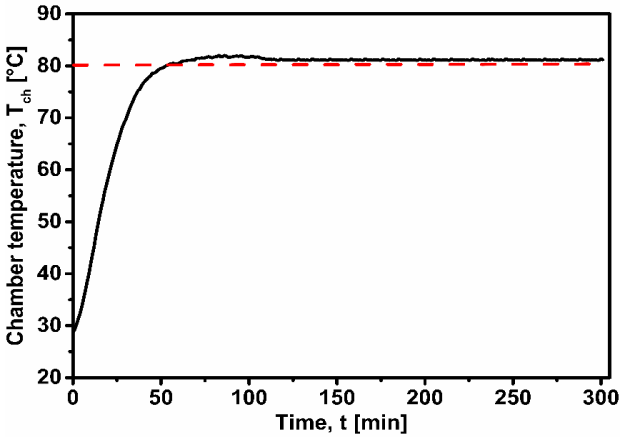

Figure 42. Experimental profile of the controlled temperature at 80°C.

Figures 43, 44, and 45 show the measured control signal delivered to the valve. It can be seen from the figures that there is no magnification of the control signal in all the tests. It has well remained in the linear zone of the subsystem (S1) between 5.3 mA and 8 mA. The control signal is smooth which is highly recommended for the valve control to prevent it from damage.

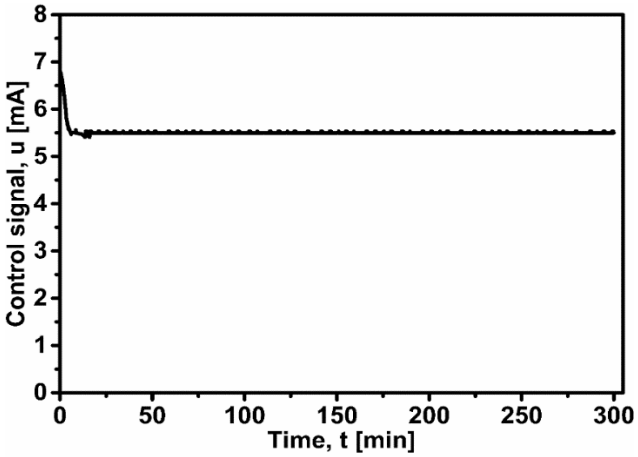

Figure 43. Control signal of the proportional valve for a temperature control test at 60°C.

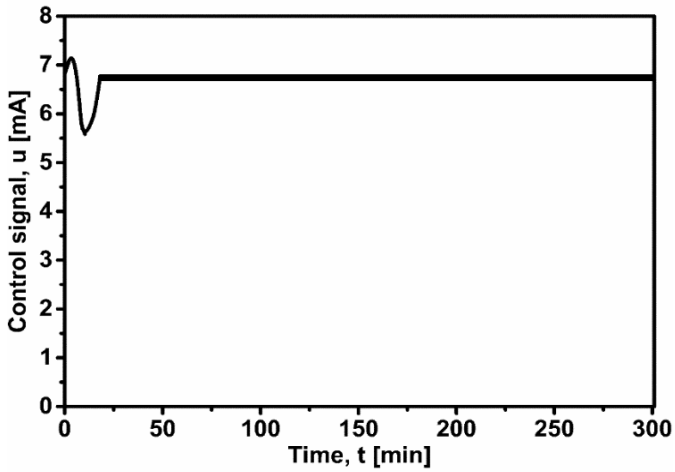

Figure 44. Valve control signal for a temperature control test at 70°C.

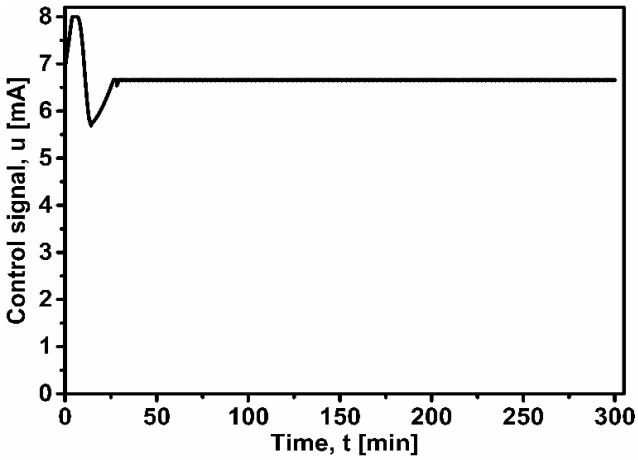

Figure 45. The control signal of the proportional valve for temperature control at 80°C.

Figures 46a,46b, 47a,47b, and 48a,48b shows the calculated reference gas flows and the measured ones for the temperature control at 60°C, 70°C, and 80°C, respectively. It can be observed from these figures that the measured gas flow tracked well the reference one in the

steady-state with slight variation in the transitory state. For the temperature control at 60°C, the consumed gas flow by the burner decreases from approximately 13.6 lt/min to reach 5.3 lt /min in the steady-state. For temperature control at 70°C, the measured gas flow is well maintained at the reference one of 6.2 lt/min in the steady-state while for temperature control at 80°C, the consumed gas flow is 14.6 lt/min at beginning of the experiment then it started to decrease until it stabilizes at 6.5 lt/min for maintaining the chamber temperature at the desired value.

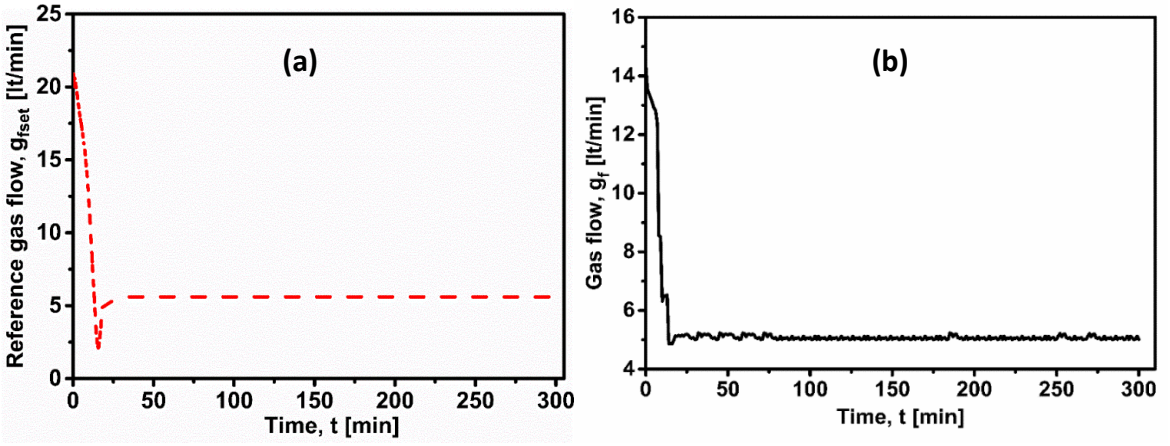

Figure 46. Consumed gas flow profile for temperature control at 60°C; (a) the calculated gas flow; (b) Measured consumed gas flow.

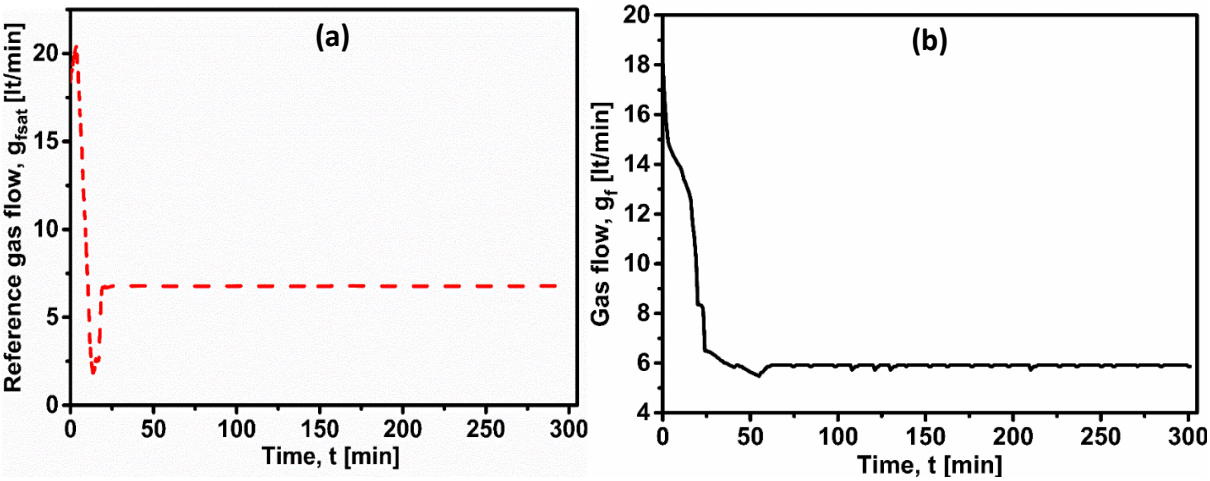

Figure 47. Consumed gas flow profile for temperature control at 70°C; (a) the calculated gas flow; (b) Measured consumed gas flow.

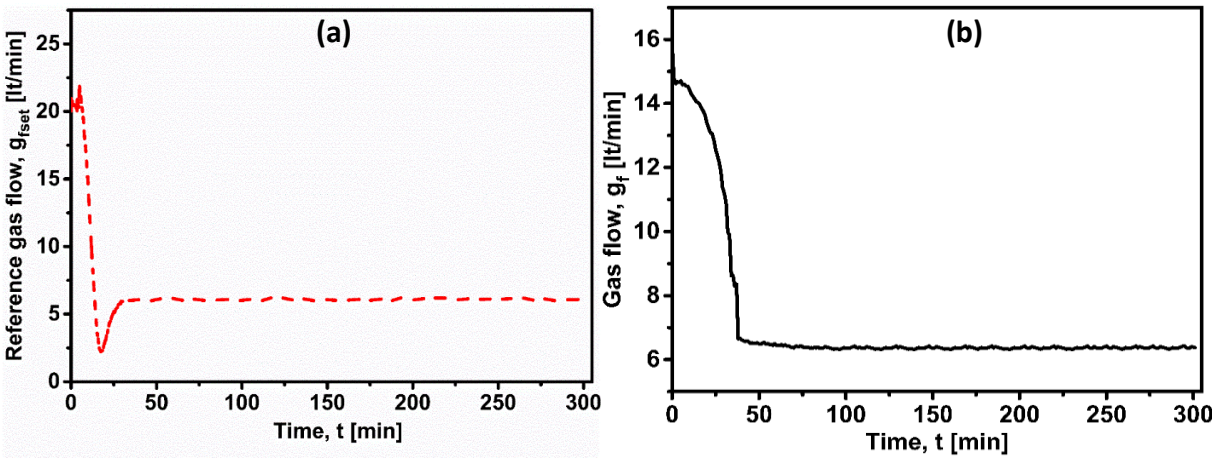

Figure 48. Consumed gas flow profile for temperature control at 80°C; (a) the calculated gas flow; (b) Measured consumed gas flow.

4.4.2. Perturbation rejection test

Within the drying process, an abrupt external perturbation could be occurred in the level of gas flow by opening manually the gas bottle or the proportional valve. To test the performance of the cascade control structure towards this unexpected perturbation, the temperature inside the drying chamber is controlled at 60°C. The experimental tests were conducted on a cloudy day. The test lasted 8 hours of operation starting from 3 pm to 11 pm. The climatological conditions during the day of experiments are presented in Table 7. During the dryer operation in steady-state, abrupt variations of the gas flow are occurred manually by the user at (t= 133 min, t = 237 min, and t = 284 min). The perturbations lasted for about 2 minutes. Figure 49 shows the temperature profile inside the drying chamber, while figure 50 depicts the gas low profile during the drying operation. It can be seen from both figures that the gas flow perturbation is rapidly rejected by the inner loop without affecting chamber temperature. It can be deduced from the obtained results that the developed control approach showed a good ability to recover the normal performances and to cancel the effect of perturbations.

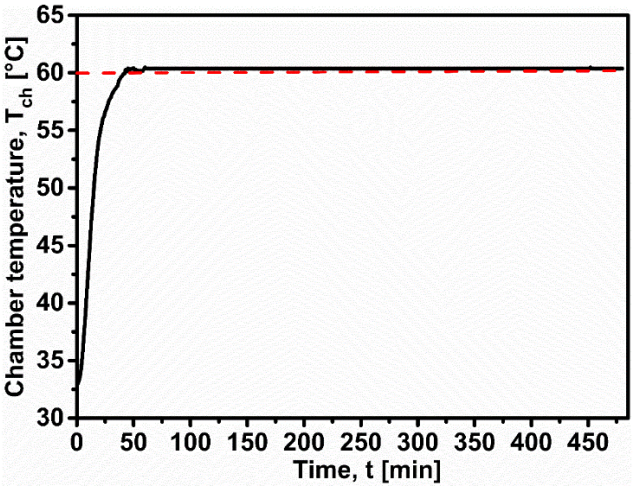

Figure 49. Profile of the drying chamber temperature.

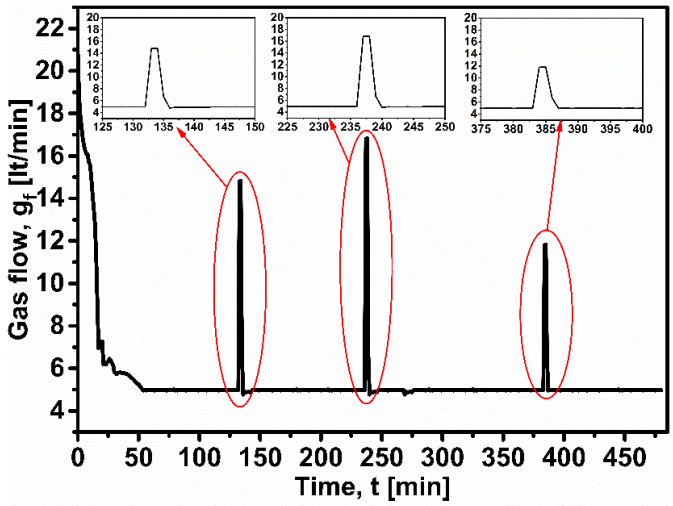

Figure 50. Measured profile of the consumed gas flow including perturbances.

Table 7. Climatological conditions during the experiments for the perturbation test.

Day of experiment	November, 11th, 2021
Average ambient temperature	22 °C
Wind speed	Max: 8 km/h Min: 1.6 km/h

5. Conclusions

In this attempt, the temperature control of a hybrid solar-gas dryer at 60°C, 70°C, and 80°C has been established. In order to develop an efficient temperature controller, the hybrid dryer system has been subdivided into two subsystems named (S1) and (S2). Subsystem (S1) represented the gas actuator which is the valve and middle burner and subsystem (S2)

represented the drying chamber combined with the collector. The behavior of each subsystem has been investigated and it turned out that both subsystems' behavior is nonlinear type threshold and saturation. Given the proposed dryer structuration, a cascade control approach has been adopted for temperature control purposes. The inner loop of the cascade strategy consists of controlling the gas flow while the outer loop is designed to update the gas flow reference to be tracked by the inner loop for a given reference chamber temperature. Two nonlinear PI controllers have been designed for both loops. Simulation studies followed by experimental validation have been established to test the reliability of the proposed approach. The proposed cascade strategy has shown a good ability to satisfy the desired performance of the dryer system in terms of accuracy (steady-state error of 0.5 %, 0,28%, and 1,12%) and rapidity (with a settling time of 20 min, 18 min, and 30 min) to set the temperature at the desired value (60°C, 70°C, and 80°C), despite the non-linearity of the studied system. Hence, the cascade control strategy is suitable for solar dryers.

Acknowledgment

Thanks to IRESEN for financially support this work.

References

[1] Abhay Bhanudas Lingayata, V.P Chandramohana, V.R.K Rajua, Venkatesh Meda. A review on indirect type solar dryers for agricultural crops – Dryer setup, its performance, energy storage and important highlights. Applied energy. (2020) 258; 114005. https://doi.org/10.1016/j.apenergy.2019.114005.

[2] Vishnuvardhan Reddy Mugi, Chandramohan V.P. Energy and exergy analysis of forced and natural convection indirect solar dryers: Estimation of exergy inflow, outflow, losses, exergy efficiencies and sustainability indicators from drying experiments. Journal of Cleaner Production. (2021) 282, 124421. https://doi.org/10.1016/j.jclepro.2020.124421.

[3] Rasaq O Lamidi, L, Jiang, Pankaj B, Pathare Y.D Wang, A.P Roskilly. (2020). Recent advances in sustainable drying of agricultural produce: A review. Applied energy. (2019) 233-234, 367-385. https://doi.org/10.1016/j.apenergy.2018.10.044.

[4] El Ferouali H, Zoukit A, Zehhar N, Benkhalti F, Bouamama H, Doubabi S, Abdenouri N. Solar drying, hygroscopic equilibrium and biochemical quality of Punica granatum Legrelliae's flowers. J. Appl. Bot. Food Qual. (2018) 91, 14–23. https://doi.org/10.5073/JABFQ.2018.091.003.

[5] Sandali M, Boubekri A, Mennouche, D. Improvement of the Thermal Performance of Solar Drying Systems Using Different Techniques: A Review J.Sol. Energy Eng. (2019) 1–11. https://doi.org/10.1115/1.4043613.

[6] El Ferouali H, Zoukit A, Salhi I, El Kilali T, Doubabi S, Abdenouri. N. Thermal efficiency and exergy enhancement of solar air heaters, comparative study and experimental investigation. J. Renew. Sustain. Energy. (2018) 10, 43709. https://doi.org/10.1063/1.5039306.

[7] Zoukit A, El Ferouali H, Salhi I, Doubabi S, Abdenouri N. Takagi Sugeno fuzzy modeling of an indirect solar dryer operated in both natural and forced convection. Renewable energy. (2019) 133, 849-860. https://doi.org/10.1016/j.renene.2018.10.082.

[8] Mohammadhossein Rezaei, Mohammad Sefid, Khalid Almutairi, Ali Mostafaeipour, Hoa Xuan Ao, Seyyed Jalaladdin Hosseini Dehshiri, Seyyed Shahabaddin Hosseini Dehshiri, Shahariar Chowdhury, Kuaanan Techato, Investigating performance of a new design of forced convection solar dryer, Sustainable Energy Technologies and Assessments, (2022) 50, 101863, ISSN 2213-1388, https://doi.org/10.1016/j.seta.2021.101863.

[9] Oueslaty H, Ben Mabrouk S, Marni A.. Design and Installation of a Solar-gas tunnel dryer: Comparative experimental study of two scenarios of drying. In: Proceeding of the fifth International Renewable Energy Congress (IREC). 1–6, Hammamet, Tunis; (2014) 25-27 March, 2014. https://doi.org/10.1109/IREC.2014.6826970.

[10] Abunde Neba F, Jiokap Nono, Y. 2017. Modeling and simulated design: A novel model and software of a solar-biomass hybrid dryer Comput. Chem. Eng, (2017) 104, 128–140. https://doi.org/10.1016/j.compchemeng.2017.04.002.

[11] Zoukit A, El Ferouali H, Salhi I, Doubabi S, Abdenouri. N. Simulation, design and experimental performance evaluation of an innovative hybrid solar-gas dryer. Energy (2019) 189, 116279. https://doi.org/10.1016/j.energy.2019.116279.

[12] C.D. Constantino-Robles, J.A. Romero-Eredia, P.Y. Sevilla-Camacho, J.B. Robles-Ocampo, L. J. Sol-Montejo, J. Rodríguez-Res´endiz, B.Y. Perez-Sari˜nana. Novel hybrid solar dryer for medicinal plants: An experimental evaluation (Tithonia diversifolia Gray). Sustainable Energy Technologies and Assessments 2022. 51, 101950, ISSN 2213-1388, https://doi.org/10.1016/j.seta.2022.101950.

[13] Abdenouri N, Zoukit A, Salhi I, Doubabi S. . Thermal management of an unloaded hybrid dryer by generalized predictive control. Drying technology (2021) https://doi.org/10.1080/07373937.2021.1967374.

[14] Abdenouri N, Zoukit A, Salhi I, Doubabi S. Model identification and Fuzzy control of the temperature inside an active hybrid solar indirect dryer. Solar energy (2022). 232, 328-342. https://doi.org/10.1016/j.solener.2021.11.026.

[15] Sumit Tiwaria, Sanjay Agrawalb, Tiwaric G.N. PVT air collector integrated greenhouse dryers. Renewable and Sustainable Energy Reviews (2018). 90, 142-159. https://doi.org/10.1016/j.rser.2018.03.043.

[16] Boughali S, Benmoussa H, Bouchekima B, Mennouche D, Bouguettaia H, Bechki D. Crop drying by indirect active hybrid solar-Electrical dryer in the eastern Algerian Septentrional Sahara" (2009). Solar Energy. 83, 2223-2232.

[17] Sekyere C. K. K, Forson F. K, Adam, F. W. Experimental investigation of the drying characteristics of a mixed mode natural convection solar crop dryer with back up heater. (2016) Renewable Energy. 92, 532–542. DOI : https://doi.org/10.1016/j.renene.2016.02.020.

[18] Lopez-Vidana E.C, Mendez-Lagunas L. L, Rodriguez-Ramirez J. Efficiency of a hybrid solar-gas dryer. Solar energy (2013). 93, 23-31. https://doi.org/10.1016/j.solener.2013.01.027.

[19] Zhihua Qu; R.A. Hull; Jing Wang.. Globally stabilizing adaptive control design for nonlinearly-parameterized systems. IEEE Transactions on Automatic Control. (2006) 51(6); 1073-1079.

[20] A.E. Ariffin., N. Munro. Robust control analysis of a gas-turbine aeroengine. IEEE Transactions on Control Systems Technology (1997) 5(2); 178-188.

[21] Gian Paolo Incremona., Matteo Rubagotti., Antonella Ferrara. Sliding Mode Control of Constrained Nonlinear Systems. IEEE Transactions on Automatic Control. (2017) 62(6); 2965-2972.

[22] Salhi, I., Doubabi, S., Essounbouli, N., Hamzaoui. Application of multi-model control with fuzzy switching to a micro hydro-electrical power plant. Renewable Energy. (2010) 35(9); 2071-2079.

[23] Campos-Rodríguez A, García-Sandoval J. P, González-álvarez V. Hybrid cascade control for a class of nonlinear dynamical systems. Journal of Process Control (2019). 76, 141–154. https://doi.org/10.1016/j.jprocont.2019.02.007.

[24] Yin X, Wang X, Li S, Cai, W. Energy-efficiency-oriented cascade control for vapor compression refrigeration cycle systems. Energy (2016). 116, 1006–1019. https://doi.org/10.1016/j.energy.2016.10.059.

[25] Li C, Choudhury M. A. A. S, Huang B, Qian F. Frequency analysis and compensation of valve stiction in cascade control loops. Journal of Process Control (2014). 24(11), 1747–1760. https://doi.org/10.1016/j.jprocont.2014.09.009.

[26] Ali Etem Gürel, Ümit Ağbulut, Alper Ergün, İlhan Ceylan, Adnan Sözen, Azim Doğuş Tuncer, Ataollah Khanlari, A detailed investigation of the temperature-controlled fluidized bed solar dryer: A numerical, experimental, and modeling study, Sustainable Energy Technologies and Assessments, (2022) 49, 101703, ISSN 2213-1388, https://doi.org/10.1016/j.seta.2021.101703

[27] Wanxiu Xu, Chunfang Song, Zhenfeng Li, Feihu Song, Shaogang Hu, Jing Li, Guanyu Zhu, G.S. Vijaya Raghavan Temperature gradient control during microwave combined with hot air drying, Biosystems Engineering, (2018)169, 175-187, ISSN 1537-5110, https://doi.org/10.1016/j.biosystemseng.2018.02.013.

[28] Zhenfeng Li, G.S.V. Raghavan, Valérie Orsat, Temperature and power control in microwave drying, Journal of Food Engineering, (2010) 97, Issue 4, 478-483, ISSN 0260-8774, https://doi.org/10.1016/j.jfoodeng.2009.11.004.

[29] Ricardo Lemos Monteiro, Jaqueline Oliveira de Moraes, Aline Iamin Gomide, Bruno Augusto Mattar Carciofi, João Borges Laurindo, Temperature control for high-quality oil-free sweet potato CHIPS produced by microwave rotary drying under vacuum," LWT, (2022)157, 113047, ISSN 0023-6438, https://doi.org/10.1016/j.lwt.2021.113047.

[30] A.-M. Nuñez Vega, B. Sturm, W. Hofacker. Simulation of the convective drying process with automatic control of surface temperature, Journal of Food Engineering, (2016) 170, , Pages 16-23, ISSN 0260-8774, https://doi.org/10.1016/j.jfoodeng.2015.08.033.

[31] Guillermo Bejarano, David Rodríguez, José A. Alfaya, Juan D. Gil, Manuel G. Ortega, Optimization and Cascade Robust Temperature Control of a Refrigerated Chamber IFAC-PapersOnLine, (2018) 51, Issue 25, 110-115, ISSN 2405-8963, https://doi.org/10.1016/j.ifacol.2018.11.090.

[32] J.I. Lombraña, R. Rodríguez, U. Ruiz, Microwave-drying of sliced mushroom. Analysis of temperature control and pressure, Innovative Food Science & Emerging Technologies,

(2010) 11, Issue 4, 2010, 652-660, ISSN 1466-8564, https://doi.org/10.1016/j.ifset.2010.06.007.

[33] Josenalde B. Oliveira, Smooth Adaptive Robust Temperature Control of a Seed Drying System, IFAC Proceedings, (2013) 46, Issue 18, 6-11, ISSN 1474-6670, ISBN 9783902823441, https://doi.org/10.3182/20130828-2-SF-3019.00012.

[34] Feng Jian-qin, Kang Guo-ping, Chen Zhi-wu, Zheng An-ping, Wei Yun-bing, Cui Guang-zhao, "Present Research Situation and Trend of Temperature Measurement and Control Technology for Dry-type Transformers, Procedia Environmental Sciences, (2011)11, Part A, 398-405, ISSN 1878-0296, https://doi.org/10.1016/j.proenv.2011.12.064.

[35] Abdenouri N, Zoukit A, Salhi I, Doubabi S. Effect of burner's configuration on the temperature profile inside an innovative solar-gas dryer: Numerical and experimental investigations, Sustainable Energy Technologies and Assessments, (2022) 49, 101690. https://doi.org/10.1016/j.seta.2021.101690.

[36] Jul-Ki Seok. "Frequency-Spectrum-Based Antiwindup Compensator for PI-Controlled Systems" IEEE Transactions on Industrial Electronics (2006), 53 (6), 1781-1790. https://doi.org/10.1109/TIE.2006.885118.

[37] Lucas Vizzotto Bellinaso, Henrique Horst Figueira, Mauro Fernando Basquera, Rodrigo Padilha Vieira, Hilton Abílio Gründling, Leandro Michels. Cascade Control With Adaptive Voltage Controller Applied to Photovoltaic Boost Converters. IEEE Transactions on Industry Applications (2019) 55(2), 13. https://doi.org/10.1109/TIA.2018.2884904.

[38] Zhiping Fan, Zhengyun Ren, Angang Chen. A Modified Cascade Control Strategy for Tobacco Re-Drying Moisture Control Process With Large Delay-Time. IEEE Access (2020). 8(1). https://doi.org/10.1109/ACCESS.2019.2960192.

[39] Garrido R, Díaz A. Cascade closed-loop control of solar trackers applied to HCPV systems. Renewable Energy (2016), 97, 689–696. https://doi.org/10.1016/j.renene.2016.06.022.